Carderock Division
Naval Surface Warfare Center
Bethesda, MD 20084-5000

NSWCCD-61-TR—1999/07 March 1999

Survivability, Structures, and Materials Directorate
Technical Report

The Influence of Localized Plasticity and Crack Tip Constraint in Undermatched Welds

by

Gerard P. Mercier

NSWCCD-61-TR—1999/07 The Influence of Localized Plasticity and Crack Tip Constraint in Undermatched Welds

REPORT DOCUMENTATION PAGE

Form Approved
OMB No. 0704-0188

1. AGENCY USE ONLY (Leave blank)	2. REPORT DATE	3. REPORT TYPE AND DATES COVERED
	March 1999	Final

4. TITLE AND SUBTITLE
The Influence of Localized Plasticity and Crack Tip Constraint in Undermatched Welds

5. FUNDING NUMBERS
PE 602234N
98-1-6140-254

6. AUTHOR(S)

7. PERFORMING ORGANIZATION NAME(S) AND ADDRESS(ES)
Naval Surface Warfare Center
Caderock Division
9500 MacArthur Blvd.
West Bethesda, MD. 20817-5700

8. PERFORMING ORGANIZATION REPORT NUMBER
NSWCCD-61-TR-1999/07

9. SPONSORING/MONITORING AGENCY NAME(S) AND ADDRESS(ES)
Office of Naval Research
Ballston Center Tower One
800 North Quincy Street
Arlington, VA. 22217-5660

10. SPONSORING/MONITORING AGENCY REPORT NUMBER

11. SUPPLEMENTARY NOTES

12a. DISTRIBUTION/AVAILABILITY STATEMENT

12b. DISTRIBUTION CODE
Distribution Code A

13. ABSTRACT (Maximum 200 words)

Four weldments of varying levels of weld joint to baseplate strength (mis-match) were examined to determine the effects of this ratio on fracture performance. Cracks were placed within the weld metal at several ratios of weld fusion margin. This margin is defined as the ratio of crack tip proximity to the weld fusion line and crack length (L_{crk}/a). Finite element studies were then performed on each variation of weld fusion margin and mis-match level to determine the crack driving force not accounted for in a typical fracture analysis, which assumes monolithic, homogenous weld metal specimens and ignores the weld/baseplate interaction. Assuming homogenous weld metal specimens results in J-R curves that exhibit markedly different crack growth resistance behavior depending on crack tip proximity to the weld fusion line. Once local plasticity and the additional constraint caused by the weld/baseplate interface are included in the analysis, fracture behavior is independent of crack tip proximity to the fusion line up to and slightly beyond initiation. Errors in fracture toughness at weld fusion margins greater than or equal to 1.5 are less than 10% and can reasonably be ignored. Errors at smaller values of L_{crk}/a are considerable, and effects of local plastic deformation and constraint must be accounted for in the fracture analysis. Furthermore, uncorrected estimates of initiation toughness (J_{IC}) in specimens where the weld fusion margin is less than 1.5 results in overly conservative estimates. The percentage of weld mis-match was found not to be a major factor in determining either crack growth resistance or crack initiation behavior. An increased propensity toward unstable fracture was observed in specimens with smaller L_{crk}/a ratios. This effect may be attributed to a local microstructural defect and requires further study.

14. SUBJECT TERMS
Fracture Testing, SE(B), Constraint, Plastic Eta Factor, Local Plasticity, Short Cracks, Welds, Undermatching, J-R Curves, h/W Effects, Weld Joint Geometry, Gamma Factor

15. NUMBER OF PAGES
48

16. PRICE CODE

17. SECURITY CLASSIFICATION OF REPORT	18. SECURITY CLASSIFICATION OF THIS PAGE	19. SECURITY CLASSIFICATION OF ABSTRACT	20. LIMITATION OF ABSTRACT
Unclassified	Unclassified	Unclassified	Unclassified

Table of Contents

List of Figures

List of Tables

Abstract

Four weldments of varying levels of weld joint to baseplate strength (mis-match) were examined to determine the effects of this ratio on fracture performance. Cracks were placed within the weld metal at several ratios of weld fusion margin. This margin is defined as the ratio of crack tip proximity to the weld fusion line and crack length (L_{crk}/a). Finite element studies were then performed on each variation of weld fusion margin and mis-match level to determine the crack driving force not accounted for in a typical fracture analysis, which assumes monolithic, homogenous weld metal specimens and ignores the weld/baseplate interaction. Assuming homogenous weld metal specimens results in J-R curves that exhibit markedly different crack growth resistance behavior depending on crack tip proximity to the weld fusion line. Once local plasticity and the additional constraint caused by the weld/baseplate interface are included in the analysis, fracture behavior is independent of crack tip proximity to the fusion line up to and slightly beyond initiation. Errors in fracture toughness at weld fusion margins greater than or equal to 1.5 are less than 10% and can reasonably be ignored. Errors at smaller values of L_{crk}/a are considerable, and effects of local plastic deformation and constraint must be accounted for in the fracture analysis. Furthermore, uncorrected estimates of initiation toughness (J_{IC}) in specimens where the weld fusion margin is less than 1.5 results in overly conservative estimates. The percentage of weld mis-match was found not to be a major factor in determining either crack growth resistance or crack initiation behavior. An increased propensity toward unstable fracture was observed in specimens with smaller L_{crk}/a ratios. This effect may be attributed to a local microstructural defect and requires further study.

Administrative Information

The work performed herein was sponsored by the Office of Naval Research 6.2 Ship and Submarine Materials Technology Block program managed by Dr. William Messick, CDNSWC (0115). The effort was conducted under program element 602234N, work unit 1-6140-254-10 and was supervised by Mr. T. W. Montemarano, Head, Fatigue and Fracture Branch (Code 614).

Introduction

Established standards typically require welded structures be composed of a weld metal of higher strength than the joined baseplate [1, 2]. Traditional U.S. Navy requirements specify weld consumables must have a higher yield strength than the base metal [3]. The assumption in this policy is that the weld metal is more apt to have defects such as porosity, slag entrapment, lack of fusion or other planar and/or volumetric discontinuities. Overmatching (using higher strength weld metal) shields these defects from plastic strain by shunting plasticity into the lower strength baseplate. The baseplate material is generally more ductile and has more consistent properties and fewer defects, lessening the likelihood of fracture. However, as the strength of the baseplate steel increases, overmatching becomes problematic. Developing weld consumables of even higher strength while retaining good weldability and toughness is difficult and expensive. Extensive preheat and interpass requirements to prevent hydrogen embrittlement in the higher strength consumable expend time and energy. Furthermore, the level of overmatch within a weld system is not assured [4, 5]. Undermatch welding (using lower strength weld consumable) allows lower preheat and interpass requirements and higher heat inputs. These changes increase productivity by increasing the weld metal deposition rate [6]. However, undermatching, unlike overmatching, does not protect the weld from strain. While the fracture toughness of the undermatched consumable may be better than the baseplate, undermatching focuses strain within the weld, potentially increasing the risk of fracture.

In an overmatched system the lower yield baseplate generally shields a crack from excessive strain thus lowering the local stress/strain fields and crack driving force (J).

Conversely, an undermatched system will concentrate the strain within the weld metal and raise the local stress/strain fields and J [7, 8, 9]. While there are special cases where the weld joint geometry can be ignored and J can be calculated using just weld metal or base metal properties [10], in most cases the proximity of the weld/base metal interface has a large influence on crack driving force [7-9]. This is expected since J is defined as a path independent contour integral [11]. Path independence of J is lost as soon as the contours are calculated across the weld/baseplate interface. Treatment of welded specimens as monolithic, single materials certainly invalidates the path independence of J and brings into question the validity of the measurement.

However, treatment of welded structures and specimens using just weld metal material properties and ignoring the weld geometry has been shown to be of value [12, 13]. Still, these global estimates do not account for the changes in stress states or variation in constraint at the crack tip in a mis-matched weld. Various authors have noted this effect and determined that undermatching increases the level of stress triaxiality or constraint at the crack while overmatching decreases it [14, 15]. Furthermore, the geometry of the welded joint and proximity of the crack to the weld fusion line also contribute to the level of crack tip constraint [15, 16, 17]. With these studies in mind an investigation of the fracture behavior of undermatched weld systems was conducted using short crack single edge notched bend specimens. An effort was made to characterize the crack driving force at the crack tip by including constraint effects of the weld/baseplate interface and any local plasticity not usually account for in typical analysis of short crack single edge notched bend specimens [18, 19].

Finite element models of the test weldments in this study were constructed to examine the crack driving force and the effects of crack proximity to the fusion line. The weld fusion margin characterizes the proximity of the crack to the weld/baseplate fusion line and is defined as the ratio of crack tip distance to the weld fusion line (L_{crk}) to the crack length (a), L_{crk}/a. Prior studies have indicated that crack growth resistance behavior is sensitive to this ratio (L_{crk}/a) [20]. Tregoning's study [20] indicated that as the weld fusion margin decreased, constraint increased, driving the crack growth resistance curve (J-R curve) down. He suggested that the global treatment of the specimens as monolithic weld metal altered the resistance curves of specimens with small weld fusion margins by not including the effects of constraint and local crack tip deformation. Results from Burstow et al. [16] seem to agree with Tregoning's assessment and show that self similar stress fields forward of the crack tip are obtained by normalizing the load parameter by the weld height. Other authors [12, 13] have shown that homogenous equations work up to J levels of 350 kJ/m^2. However, above this level error in the fracture toughness calculation occurred. This study examines the effects of both constraint caused by weld geometry and mis-match level and determines the error associated with using global measurements while assuming homogenous weld metal properties.

New coefficients (η-factors) are developed to relate the crack driving force at the crack tip within the undermatched weld to the globally measured plastic work done to the specimen during testing. Comparisons of specimen analysis using these η-factors and analysises assuming all weld metal properties in a homogenous specimen are shown.

Weld Production and Material Characterization

Joint Design

Two standard military welding consumables, Mil-70s and Mil-100s, were used to fabricate four two-inch thick weldments. The consumables have nominal ultimate tensile strengths of 480 MPa (70 ksi) and 690 MPa (100 ksi). One weldment used the Mil-70s and the remaining three used Mil-100s. All four plates used typical naval steel, HY-100, with a nominal yield strength of 725 MPa, creating three approximately 10% undermatched and one 38% undermatched weld systems. Specified chemical compositions for these three materials are summarized in Table 1and are given in more detail in references 21 and 22.

Material	*C*	*Mn*	*P*	*S*	*Si*	*Ni*	*Cr*	*Mo*	*Va*	*Ti*	*Cu*	*Ar*	*Sn*	*An*	*Zr*	*Al*
HY-100	0.10-0.22	0.10-0.45	0.02	.002-0.02	0.12-0.38	2.67-3.57	1.29-1.86	0.27-0.63	0.03	0.02	0.25	0.025	0.03	0.025	—	—
Mil-70s	0.07-0.19	0.90-1.40	0.025	0.035	0.40-0.70	—	—	—	—	—	—	—	—	—	—	—
Mil-100s	0.08	1.25-1.80	0.012	0.008	0.20-0.55	1.40-2.10	0.30	—	0.10	0.10	—	—	—	—	0.10	0.10

Table 1
Specified Chemical Composition

Three different weld joint geometries were selected for study, a single 45° vee with no root gap, a single 45° vee with a 1.25-cm root gap and a symmetric double 60° vee with no root gap. The double vee joint had two permutations, one 38% undermatched with Mil-70s and the second 11% undermatched with Mil-100s. The four different weld systems were chosen to isolate effects of weld joint undermatching and study the concentration of deformation within the weld material. Each weldment is summarized in Table 2 with the weld joint geometry shown in Figure 1.

Weld Metal	ID	Geometry	Root Gap	L_{crk}/a	% Mismatch
MIL-70s	HBA	Double Vee	None	1.35	-38
MIL-100s	HBB	Double Vee	None	1.5	-11
MIL-100s	HBC	Single Vee	1.25 cm	0.75 / 3.3	-6
MIL-100s	HBD	Single Vee	None	0.20 / 2.9	-13

Table 2
Weldment Parameters

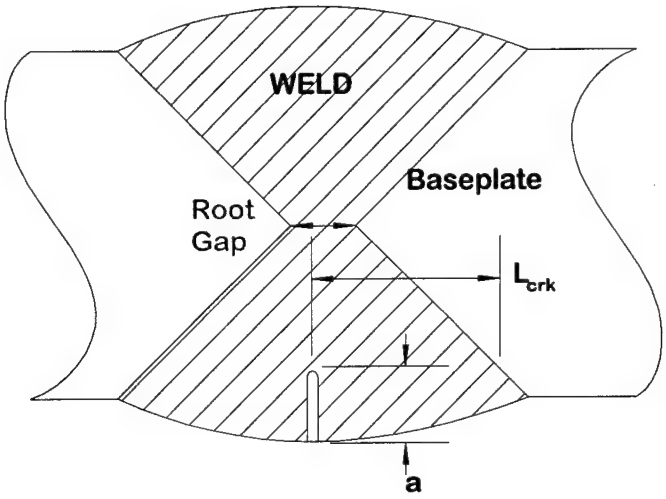

Figure 1
Weld Joint Geometry

Gas metal arc welding was used for all weldments with preheats and interpass temperatures of 175°C. Heat inputs for the Mil-70s weld ranged from 2.5-2.75 kJ/mm and heat inputs for the Mil-100s welds was 3.15 kJ/mm. The parameters were chosen to create consistent weld metal properties and do not fall within the allowable ranges for production welds. The welds were flipped regularly during production to alleviate residual stresses and weldment deformation and radiographs were taken after completion. Specimens were removed from areas where radiographs showed no or inconsequential indications.

Specimen Removal and Weld Characterization

Charpy V-notch specimens were taken transversely (T-S orientation) from both the top and bottom of each weld with the notch centered within the weld metal. Testing was conducted in accordance with ASTM E23 [23] to compare variability among weldments and determine upper and lower transition regions. Within the transition region a minimum of five specimens were tested at each temperature. Upper and lower shelf energies were measured with three specimens at each temperature.

A minimum of four 0.505 inch all weld tensile specimens were removed from each weldment (L orientation), two from the weld top and two from the bottom. Specimens from the root gap of single vee weldments were removed far enough away from the weld surface to ensure an all weld specimen. The specimens were tested in accordance with ASTM E-8 [24] at –2°C to provide tensile data at our subsequent fracture test temperature.

Six short crack (a/W=0.15) single edge bend SE(B) specimens were removed from each double vee weldment in the T-S orientation with the notch tip centered in the weld metal. The notches on the six specimens were located so that the crack sampled material from the top side of the weld in three specimens and the bottom on the remaining three. Ten short crack SE(B) specimens were removed from each single vee weldment in the T-S orientation with the notch tip centered in the weld metal. The notches on the ten specimens were located so that the crack sampled material from the top side of the weld in five specimens and the bottom on the remaining five.

Charpy Testing

Figure 2 contains all the Charpy V-notch energies (CVE) from each weld specimen. Plotted are the means for each temperature and bars indicating 95% confidence intervals. The plot shows limited variability of the Mil-100s consumable within transition and lower shelf and none of significant statistical importance. Surprisingly, the largest inconsistency occurs at upper shelf energy values. An analysis of the variance using a 95% confidence criterion shows that significant statistical difference do not occur between HBC and HBB Mil-100s welds at upper shelf CVEs. The Mil-70s weld metals shows considerably lower CVE at all temperature except upper shelf where it is equivalent to the Mil-100s. While CVE values from these four weldments satisfy requirements set in reference [21], past testing of production welds indicates that upper shelf behavior should occur prior to 0°C [25].

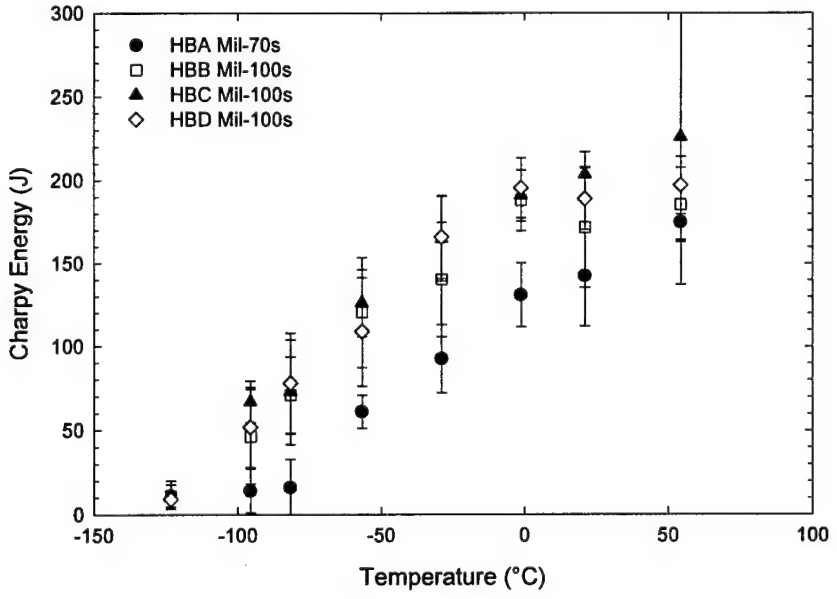

Figure 2
Charpy Data

Tensile Testing

Weld tensile testing was conducted at –2°C to provide yield and ultimate tensile strength at the same temperature used during fracture testing. Table 3 summarizes the reduction in area, strain to failure and percent undermatch for each weldment.

ID	e_f (%)	Reduction in Area (%)	σ_{ys} (MPa)	σ_{uts} (MPa)	σ_{FL} (MPa)	% Mismatch
HBA	29	70	450	600	525	-38
HBB	26	70	645	730	687.5	-11
HBC	25	71	680	740	710	-6
HBD	27	71	630	700	665	-13

Table 3
Basic Tensile Properties of Weldments

Strain was recorded past maximum load for all specimens. This data was then used to generate true stress/strain curves, shown in Figure 3, for finite element analysis. Portions of the curves beyond 12% true strain were extrapolated linearly to avoid convergence problem in the numerical analysis. The HY-100 data was developed from compression tests from an Office of Naval Research platform structural materials program. No further analysis on weld joint tensile performance was conducted as a previous report [20] dealt extensively with weld joint strength and structural performance.

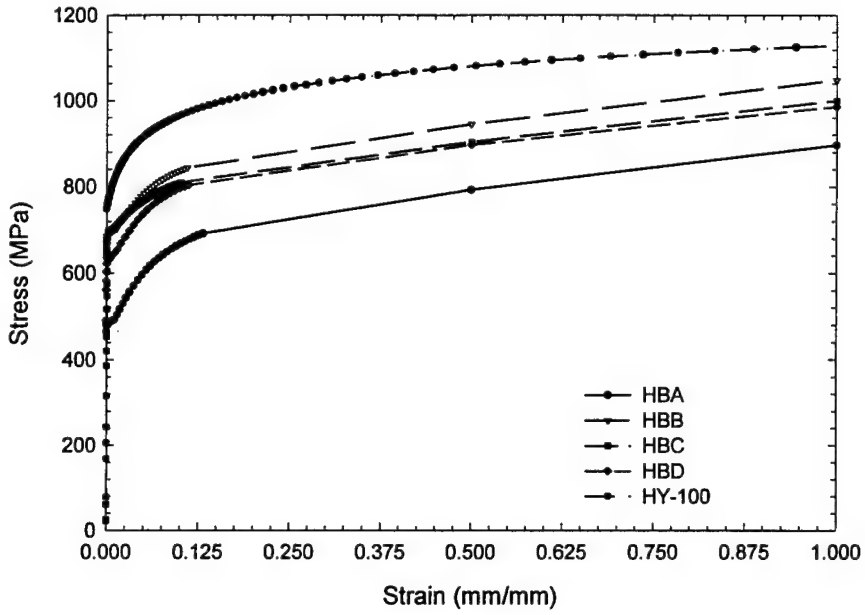

Figure 3
True Stress/Strain Data Used in Finite Element Analysis

Short Crack Single Edge Notched Bend Test Procedures

All SE(B) specimens underwent one cycle of reverse precompression in 4 point bending to 50% of limit load based on flow properties of the weld metal. Reverse precompression homogenizes crack tip residual stress fields thereby allowing straight crack fronts to grow under cyclic fatigue loading. This technique has proven effective for the T-S orientation in previous tests [20] and resulted in consistently straight precracks in this test series. ASTM 1820-96 requires that deviation from the average of nine physical precrack length measurements be less than 5%. For short crack specimens, a/W=0.15, this requirement is overly stringent and disqualified precracks with a deviation greater than 0.4 mm from the average. Several precracks did not meet this strict requirement. The precrack in Figure 4 varied by 6.5% from the average physical measurement and is technically invalid. However, analysis of thumbnailed or circular arced crack fronts with radii equal to three times specimen thickness show almost constant stress intensity (K_I)

values along the crack front [26]. These K_I values are consistent with standard calculations of stress intensity using straight cracks [27]. Therefore, specimens with precracks exhibiting shapes consistent with the above statements are included in this study.

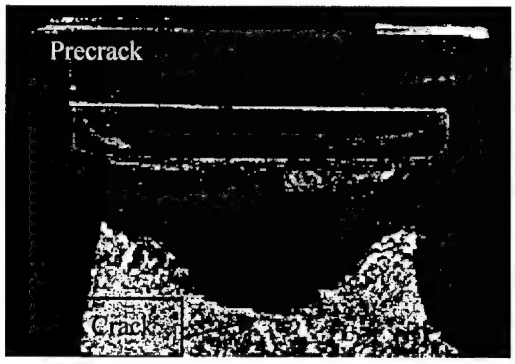

Figure 4
Precrack with Length Deviations Greater than ASTM Specifications

While precompression effects on toughness have been shown to decrease plane strain fracture toughness (K_{IC}) [28, 29] other studies indicate that this method [30] as well as a high R ratio method [31] method have little effect on toughness if ductile tearing is the mode of failure. All specimens in this study exhibited substantial ductile crack growth negating any effect induced by the reverse precompression. Further, since all specimens were deformed at a consistent level during precompression any residual stress effects would also be consistent making comparisons appropriate.

After homogenization of residual stresses was complete, fracture toughness testing was performed in accordance with reference [32] where appropriate. Single specimen unloading compliance tests where conducted on a computerized data acquisitions system in a 250 kN screw driven test frame. A compliance equation for short crack SE(B) specimens was found in [19] and is valid for $0.05 \leq a/W \leq 0.45$. Joyce

has shown that as a/W decreases, limit load increases, allowing for deeper unloads during testing and only slightly reducing the resolution of the compliance measurement [33]. Loadline displacement (Δ_{LL}) was measured directly on the specimen via a flex bar. This method avoids errors due to brinnelling and load train compliance estimates.

J Estimation

Several authors [18, 19, 34] have developed equations for applied J in a short crack SE(B) specimen with the general format:

$$J = J_{el} + J_{pl} = \frac{K^2}{E'} + \left[J_{pl(i-1)} + \frac{\eta_{(i-1)}}{b_{(i-1)}} \left(\frac{A_{pl(i)} - A_{pl(i-1)}}{B_N} \right) \right] * \left[1 - \lambda_{(i-1)} * \frac{a_{(i)} - a_{(i-1)}}{b_{(i-1)}} \right] \quad (1)$$

Where:

K = the elastic stress intensity factor,
E' = the plane strain elastic modulus,
$A_{pl(I)}$ = the area under the load versus plastic load line displacement curve at increment *i*,
B_N = the net specimen thickness,
a_I = the crack length at increment *i*,
b_i = the remaining specimen ligament at increment *i*,
W = the specimen width,
η_{pli} = the plastic eta factor at increment *i*,
γ_i = the gamma function at increment *i*.

$$\gamma_i = \left[\eta_{pli} - 1 - \frac{b_i \eta'_{pli}}{W \eta_{pli}} \right] \quad (2)$$

However, their analysis assumed a monolithic, homogeneous material. A cracked specimen composed of more than one material is not defined solely by the geometry of the specimen or depth of the crack. Crack tip stress fields are also controlled by both weld geometry and degree of mismatch [13-15]. Furthermore, it has been shown that the distance from the crack tip to the weld/baseplate interface has a pronounced effect on

crack tip stresses [15-17]. Typical test procedures and analysis do not account for the increased driving force created at the crack tip as the baseplate metal constrains the deformation within the weld. Prior work has shown that homogenous J equations are accurate for $J \approx 350$ kJ/m^2 [12, 13]. However, above this level dramatically different tearing resistance behaviors have been observed due to the inability of the homogenous analysis technique to account for the crack tip local plasticity [20].

Gordon and Wang [13] developed η_{pl}-factors for straight butt weld deep crack SE(B) specimens (a/W=0.5) with weld height to width ratios, shown in Figure 5, ranging from 0.05 to 2.

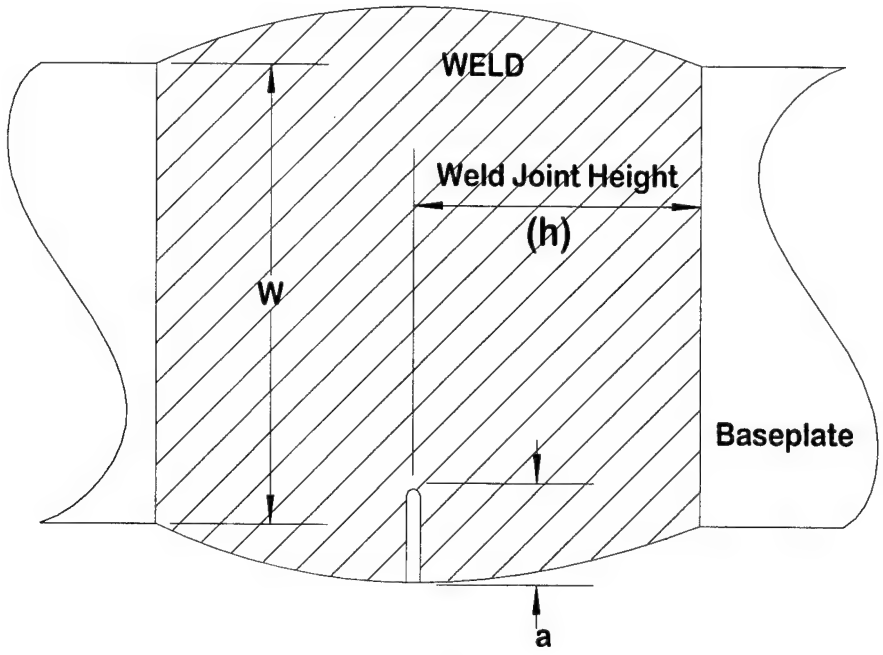

Figure 5
Weld Joint Defined by Gordon and Wang [13]

They determined that at h/W values greater than one and also at very low values of weld joint height (h/W<0.25) specimen behaved independent of h/W. And that η_{pl} approached values similar to homogenous all weld specimen or all baseplate specimens at

these values of h/W. Between these limiting values η_{pl} increased for undermatched welds and decreased for overmatched. However, Gordon and Wang concluded that for deeply cracked welded specimens the variation in η_{pl} between weld joint heights of $0.25<h/W<1$, still provided reasonable estimations of J to within 10%.

Several authors [33, 34, 35, 36] have studied crack length and work hardening effects on homogenous SE(B) specimens. They determined that for short cracks, work hardening played a major role in the calculation of J using η_{pl}-factors. It is apparent that for short crack bend specimens, each combination of mismatch level, L_{crk}/a, and hardening characteristics must be taken into account for a correct estimation of crack driving force. To accomplish this finite element models were constructed to correct for the local plasticity or crack tip deformation not accounted for with standard analysis techniques. New plastic η-factors were calculated for Equation 1, accounting for weld mis-match, crack length and weld fusion margin effects.

Finite Element Model Verification

The commercial finite element package, ABAQUS, was used to calculate plastic J-Integral solutions for lengths ranging from a/W of 0.10 to 0.30. A typical model has 1000 to 1500 eight noded plain strain reduced integration elements with 15 to 20 elements along the two-inch width of the specimen. Mesh studies indicated that a minimum of 10 elements is required to capture variation in strain along the width of the specimen. Half symmetry was used to reduce modeling and computing times. As shown in Figure 6, loading was accomplished by applying displacement to two nodes at the specimen top surface along the symmetry plane and by simply supporting one node at the half span of the specimen. A symmetry boundary condition was applied to the elements

along the remaining ligament in the same plane that contained the crack. A keyhole with a 0.0127-mm (0.0005-inch) radius, shown in Figure 7 is used to model the crack. Typically, forty to sixty radial rings of elements surround the crack tip, gradually increasing in size from 0.00635-mm (0.00025-inch) at the keyhole to 1.27-mm (0.05-inch) at the last ring. Each ring contained 24 elements dispersed equally around the keyhole. All nodes along the keyhole radius, with the exception of the one node that was on the symmetry plane, were unconstrained to simulate blunting behavior. J values were calculated at between 15 to 30 contours to ensure path independence was maintained.

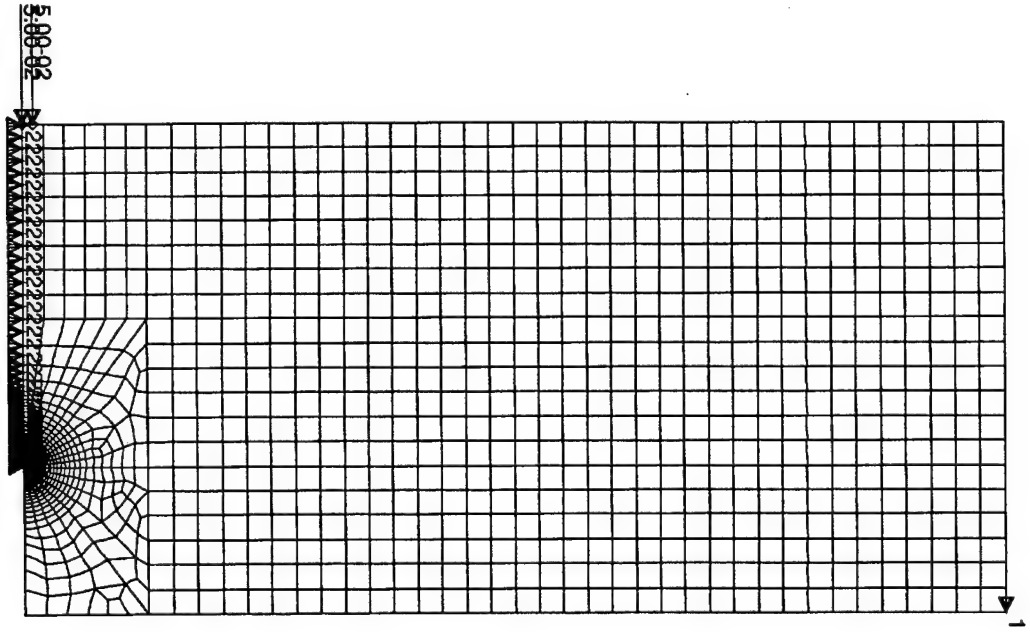

Figure 6
Loading and Mesh Design

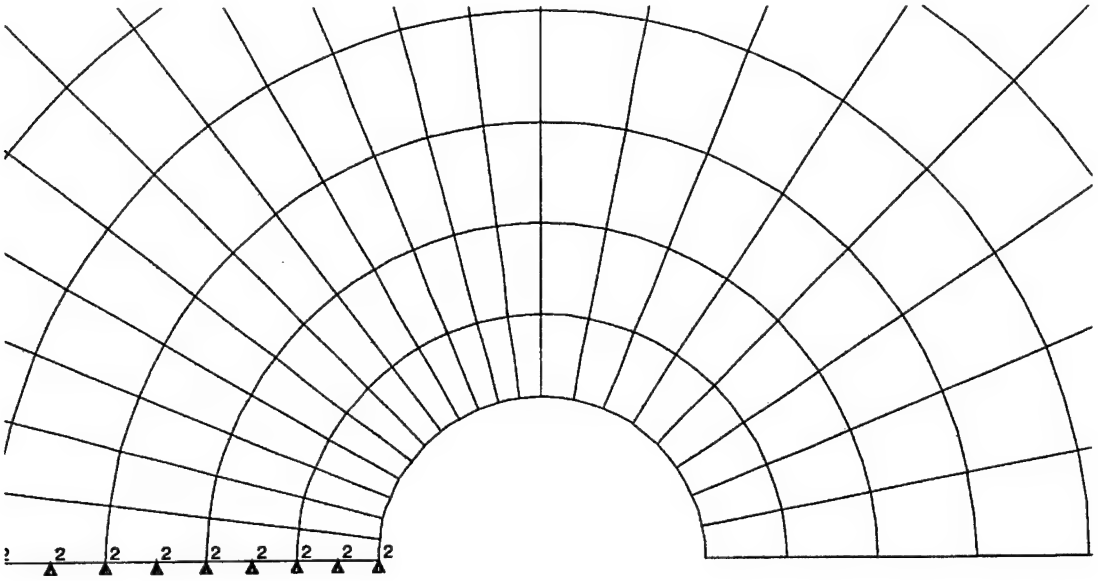

Figure 7
Crack Tip Mesh

Mesh Verification

The accuracy of the finite element model and data reduction techniques were verified by reproducing accepted solutions for homogenous SE(B)s. Three linear elastic finite element models (a/W= 0.15, 0.20, 0.30) were displaced to a loadline displacement of 1.27 mm. Load (P) and elastic J-Integral (J_{el}) values were computed at the end of each loading. The normalized compliances (BE'C) predicted from this analysis display little deviation from the predicted handbook values [37]. This result confirms that the model boundary conditions correspond to three point bending boundary conditions.

To ensure that the mesh was suitable for fracture analysis, J_{el} values were compared with values calculated by Tada [37]. J_{el} is defined as:

$$J_{el} = \frac{K^2}{E'} \qquad \text{Where } K = \sigma\sqrt{\pi a}F(a/W) \tag{3}$$

In Equation 3, F(a/W) is a geometry dependent function of normalized crack length, σ is the remote stress and a is the crack length. While J_{el} can be determined with a relatively coarse mesh, gross variation in values from the reference values would indicate a problem with crack definition or boundary conditions. Variations with handbook values were less than 1% for all three crack lengths.

Mesh refinement and crack tip geometry were verified by comparison of η_{pl} with published results from references 18 and 33. Loading and boundary conditions for all three models were maintained the same as in the previous elastic analysis. However, the plastic response of the models was defined by a Ramberg-Osgood stress/strain relationship (σ_{ys}=700 Mpa, n=10, α=0.5). Elements at the support and point of load application were defined as elastic to distribute displacements evenly and save computational time. Each loading was separated into 20 steps. At each step, load, load-line displacement and J-Integral values were determined and the plastic area (A_{pl}) and J_{pl} calculated. A_{pl} is defined by:

$$A_{pli} = \frac{(P_{i-1} + P_i)}{2}(\Delta_{i-1}^{LLpl} - \Delta_i^{LLpl}) \qquad \text{and} \qquad (4)$$

$$J_{pl} = J_{total} - J_{el} \qquad (5)$$

Where J_{el} was found using Equation 3

The plastic eta factor, η_{pl}, is defined as:

$$\eta_{pl} = \frac{J_{pl} B_N b}{A_{pl}} \qquad (6)$$

If J_{pl} is normalized by the flow stress (σ_0) and remaining ligament (b) and A_{pl} normalized by the net thickness (B_N), b and σ_0, then η_{pl} can be determined by the slope of the normalized J_{pl} vs. A_{pl} curve.

$$\eta_{pl}\frac{A_{pl}}{B_N b^2 \sigma_o} = \frac{J_{pl}}{b\sigma_o} \tag{7}$$

The normalized values of J_{pl} and A_{pl} are plotted for a/W=0.3 in Figure 8. A comparison (Table 4) of the analyses with Sumpter [18] who used the same Ramberg-Osgood stress/strain coefficients and Joyce [33] who used piecewise linear data from actual HY-100 tensile tests, confirms that the crack tip geometry, mesh refinement and data reduction techniques used are suitable and consistent.

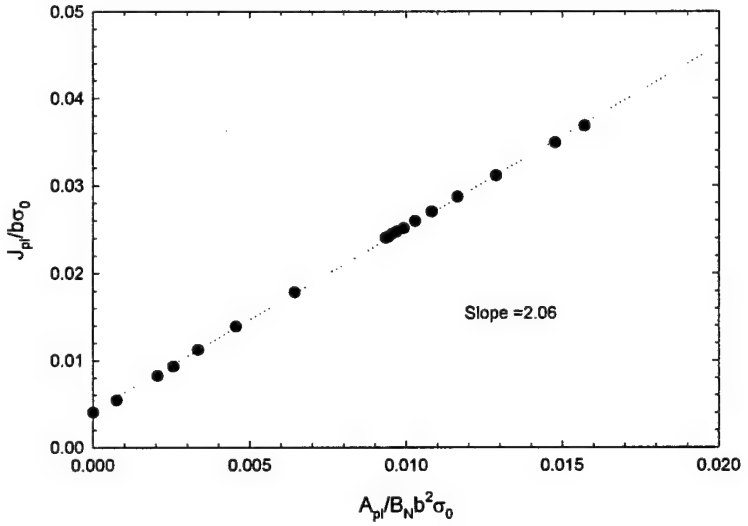

Figure 8
η_{pl} Analysis in SE(B) at a/W=0.30

a/W=	0.15	0.2	0.3
Sumpter	1.34	1.54	2
Joyce	1.6	1.82	1.89
Mercier	1.36	1.62	2.06

Table 4
η_{pl} Factors for Monolithic, Homogenous Specimen

J Analysis of Weldment Specimens

ID	Geometry	L_{crk}/a	% Mismatch
HBA	Double V	1.35	-38
HBB	Double V	1.5	-11
HBC	Single V	3.3 / 0.75	-6
HBD	Single V	2.9 / 0.2	-13

Table 5
Weldment Geometry and Mismatch Level

Once the finite element mesh was verified as accurate the models where redefined to include joint geometry and both weld and baseplate material properties. Table 5 shows the weld geometry, weld fusion margin and percent mismatch for the four weldments in this study. Plastic η-factors were developed for each unique weldment and joint design. These new plastic η-factors were then incorporated into an in house analysis code using linear curve fits to generate crack growth resistance data. The new curve fits are shown in Figure 9. All η_{pl} values of models with a weld fusion margin less than 1.5 were elevated above the homogenous (Sumpter) weld metal η_{pl}. Models with larger fusion margin values will show little deviation from the homogenous weld metal results. Models at a/W=0.30 had converged at $\eta_{pl} \approx 2.0$ where they agreed with homogenous results. However, the severity of the weld fusion margin in weldment HBD (0.2) immediately placed η_{pl} above 2.0 and increased until a/W=0.3. Further, results for

weldment HBB and the wide sides of welds HBC and HBD were nearly identical to the homogenous weld metal results of Sumpter and are plotted as HBB/Sumpter in Figure 9. Therefore, for these geometries ($L_{crk}/a \geq 1.5$) Sumpter's third degree polynomial expression is used in the subsequent analysis.

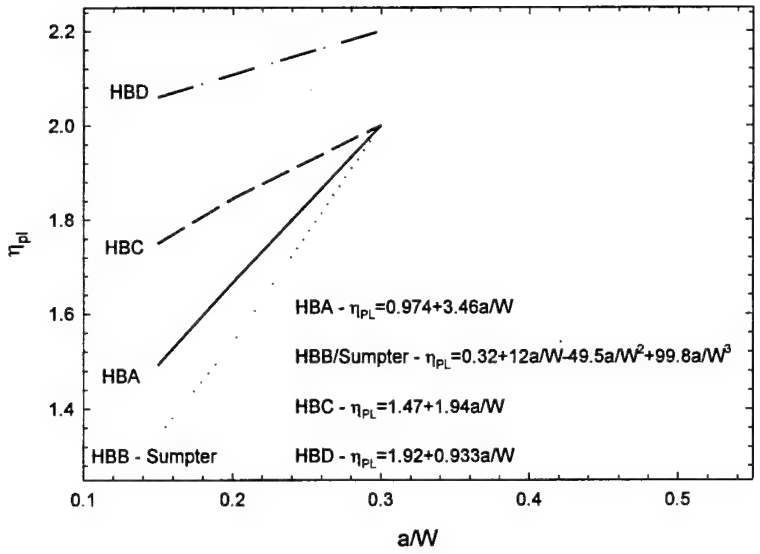

Figure 9
Curve Fits of η_{pl}-Factors for Undermatched Welds

Results and Discussion

J values were calculated for each specimen where the weld fusion margin was less than 1.5 using both the η-factors from reference 18 and the η-values from Figure 9. Comparisons of crack growth resistance and initiation were then made between the two separate analysises. Finally, initiation toughness and crack growth resistance comparisons were made on various levels of weld/baseplate mis-match and L_{crk}/a to study the effects of undermatching and joint geometry respectively.

Due to the steep slope of the initial portion of the J-R curves in these specimens, slight changes in initial estimated crack lengths (a_{oq}) result in relatively large changes in the calculated value of J_{IC}. These changes can be well within limits defined by reference 32 and still provide unacceptable changes in initiation toughness estimates. For example, a change in initial crack length of 1% in specimen HBA-5 from 7.75 to 7.67 mm results in a 25% change in J_{IC}. To avoid large inaccuracies in comparisons between analysis techniques, care was taken to set the initial crack length as close to the physically measured length as possible. This length was then maintained for each subsequent analysis.

Effect of L_{crk}/a on Initiation Toughness and the J-R Curve

The first weldment analyzed by both homogenous and local plasticity methods was HBA, Mil-70s, double vee with a weld fusion margin of 1.35. Six specimens, three from each side of the double vee, were analyzed first using homogenous weld metal properties, then reanalyzed accounting for driving force missed by the global homogenous analysis. Since the mis-match level is high (-38%), extra strain will be funneled into the weld metal and not be accounted for by the homogenous analysis. Figure 10 shows results from the two analyses and 95% confidence limits based on a power law fit through all specimen data points from each analysis. Clearly at this level of mis-match and weld fusion margin the amount of driving force missed by the homogenous weld metal analysis is minimal. A slight increase in crack growth resistance can be noted. However, the additional effort required to determine this increase is not trivial and may only be of interest to an experimentalist.

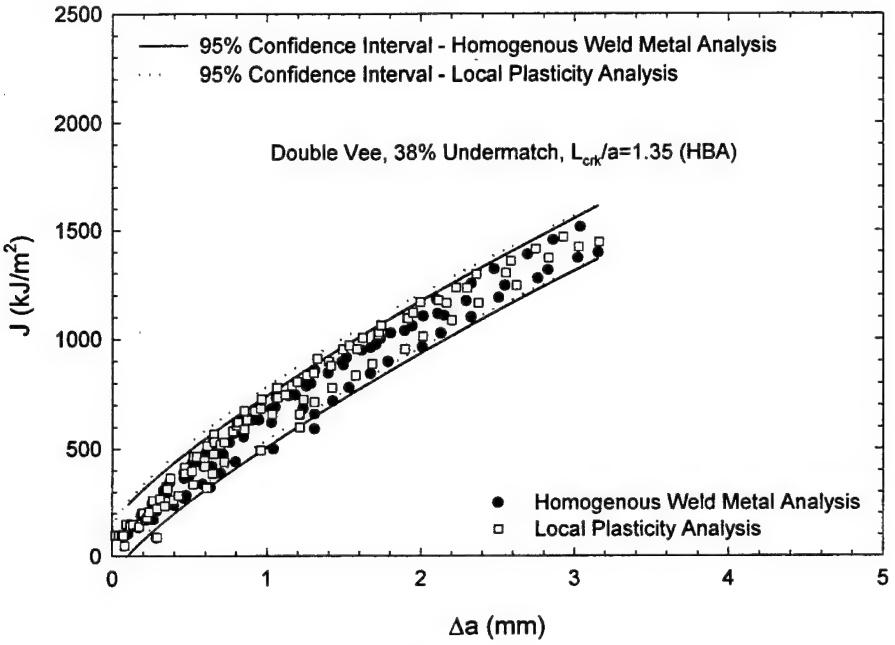

Figure 10
Crack Growth Resistance Curve for Weldment HBA

ID	*Location*	*Analysis*	*J_{IC} (lbs/in)*	*J_{IC} (kJ/m^2)*	*Valid*	*Comments*
HBA-1	TOP	Homogenous	2502	438	YES	
HBA-1	TOP	Local Plasticity	2775	486	YES	
HBA-2	TOP	Homogenous	3252	569	YES	
HBA-2	TOP	Local Plasticity	3645	638	NO	Invalid Thickness
HBA-3	TOP	Homogenous	3013	527	YES	
HBA-3	TOP	Local Plasticity	3337	584	NO	Invalid Thickness
HBA-4	BOTTOM	Homogenous	250	44	NO	Valid J_c
HBA-4	BOTTOM	Local Plasticity	250	44	NO	Valid J_c
HBA-5	BOTTOM	Homogenous	1675	293	YES	
HBA-5	BOTTOM	Local Plasticity	1848	323	YES	
HBA-6	BOTTOM	Homogenous	2623	459	YES	
HBA-6	BOTTOM	Local Plasticity	2810	492	YES	Excluding HBA-4
Average	TOP	Homogenous	2922	511	S.Dev.	67
Average	TOP	Local Plasticity	3252	569	S.Dev.	77
Average	BOTTOM	Homogenous	2149	376	S.Dev.	117
Average	BOTTOM	Local Plasticity	2329	408	S.Dev.	119

Table 6
Initiation Toughness Values for Weldment HBA

Initiation values, shown in Table 6, vary depending on specimen location (top or bottom of weld). However, the significance of this difference is difficult to quantify with

so little data. J_{IC} is elevated approximately 10% if local plasticity is accounted for in the calculation of J. As with the crack growth resistance behavior, the extra effort required to include local plasticity in the J_{IC} calculation may not be of value.

Four of the six tests in this series experienced crack growth instabilities ending the test. While three of these specimens had considerable ductile growth prior to failure, specimen HBA-4 experienced unstable growth after only 0.03 mm of crack extension and was excluded from calculations of average J_{IC} values. Zhang et al. [38] has shown that cleavage failure in multi-pass Mil-70s welds is governed by a brittle fusion line band that forms between each welding pass. Zhang et al. used stereo section fractography to determine the cleavage initiation site and show the underlying microstructure related to that site. They defined microstructural zones present in multi-pass weldments and illustrated the inherent inhomogeneity associated with a single weld bead. These zones range from a coarse columnar region that resembles a casting to several different heat affected zones whose properties depend on maximum temperature and cooling rates. One or more of these zones may act as a brittle region or weak link within the surrounding microstructure. As the crack samples this brittle area, cleavage initiation is triggered. The distance between the end of the fatigue crack and this brittle band determines the amount of ductile crack growth.

The second weldment studied was HBC, Mil-100s, single vee with weld fusion margins of 0.75 and 3.3. Ten specimens, 5 from the wide side of the single vee (L_{crk}/a=3.3) and 5 from the narrow side (L_{crk}/a=0.75) were analyzed as previously explained. Figure 11 shows the results from both homogenous analysis and the local

plasticity analysis of the narrow side of the weld. Again 95% confidence intervals are shown for each data set.

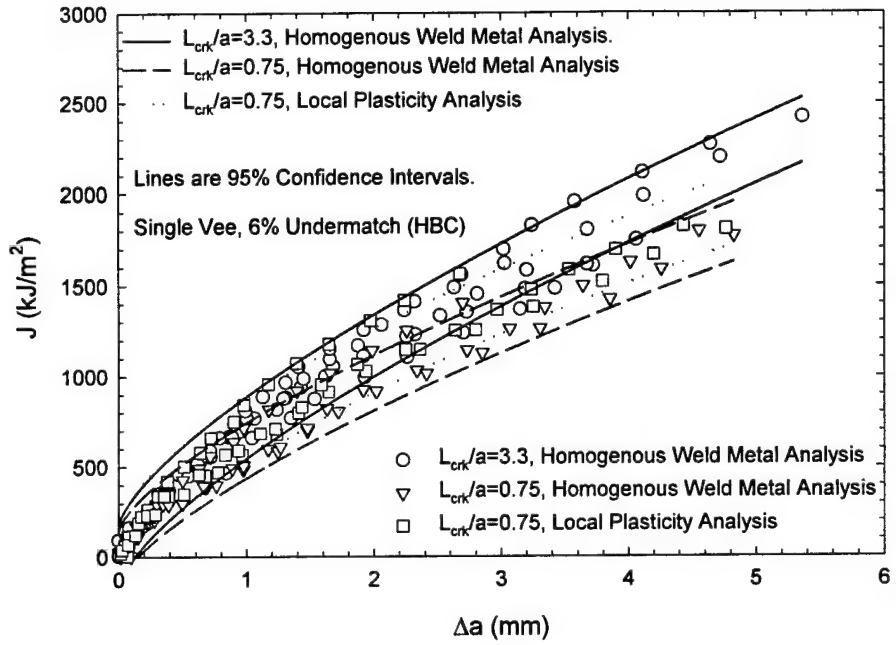

Figure 11
Crack Growth Resistance Curves for Weldment HBC

Clearly, the local plasticity analysis shifts the low weld fusion margin data onto the larger weld fusion margin curve. In fact, the confidence limits for both sets are virtually identical until J>1000 kJ/m^2. However, the homogenous weld metal analysis confidence limits deviates immediately and would indicate two separate material behaviors based on specimen location or a large increase in crack tip constraint resulting in a depressed resistance curve prior to initiation. The local plasticity confidence limits generously overlaps the large weld fusion margin data well beyond initiation. This would indicate one material behavior for this weldment and little or no effect from additional crack tip constraint.

Table 7 contains initiation values for weldment HBC using both the homogenous weld metal and local plasticity for the small weld fusion margin and homogenous only

for the larger fusion margin. Comparisons of the two homogenous analyses would indicate two separate material behaviors based on specimen location in the weld. The difference in initiation behavior between the two homogenous analyses is significant at the 95% confidence level. While comparisons of the smaller weld fusion margin analysis accounting for localized plasticity and the large weld fusion margin homogenous analysis show variations, these variations are not statistically significant at the same level. Accounting for local plasticity elevates the average initiation toughness value by slightly more than 25%. This could have a significant influence on structural design since the uncorrected value is unduly conservative.

ID	Location	Analysis	J_{IC} (lbs/in)	J_{IC} (kJ/m^2)	Valid	Comments
HBC-1	Wide	Homogenous	2697	472	YES	
HBC-2	Wide	Homogenous	2880	504	YES	
HBC-3	Wide	Homogenous	2785	487	YES	
HBC-4	Wide	Homogenous	2516	440	YES	
HBC-5	Wide	Homogenous	2570	450	YES	
HBC-6	Narrow	Local Plasticity	1712	300	YES	
HBC-6	Narrow	Homogenous	1392	244	YES	
HBC-7	Narrow	Local Plasticity	1902	333	YES	
HBC-7	Narrow	Homogenous	1589	278	YES	
HBC-8	Narrow	Local Plasticity	1913	335	YES	
HBC-8	Narrow	Homogenous	1683	295	YES	
HBC-9	Narrow	Local Plasticity	2024	354	YES	
HBC-9	Narrow	Homogenous	1432	251	YES	
HBC-10	Narrow	Local Plasticity	3279	574	YES	
HBC-10	Narrow	Homogenous	2443	428	YES	
Average	Wide	Homogenous	2690	471	S.Dev.	26
Average	Narrow	Local Plasticity	2166	379	S.Dev.	111
Average	Narrow	Homogenous	1708	299	S.Dev.	75

Table 7
Initiation Toughness Values for Weldment HBC

All of the HBC specimens in this study failed unstably after significant ductile growth. This is not unexpected given the results from Zhang et al. discussed previously.

Typically more than 3.5 mm of crack extension occurs prior to failure. The data appears to suggest that for smaller weld fusion margins the propensity for unstable failure increases. However, an analysis of the variance between the amount of ductile growth prior to cleavage failure shows no statistical significance at the 95% confidence level.

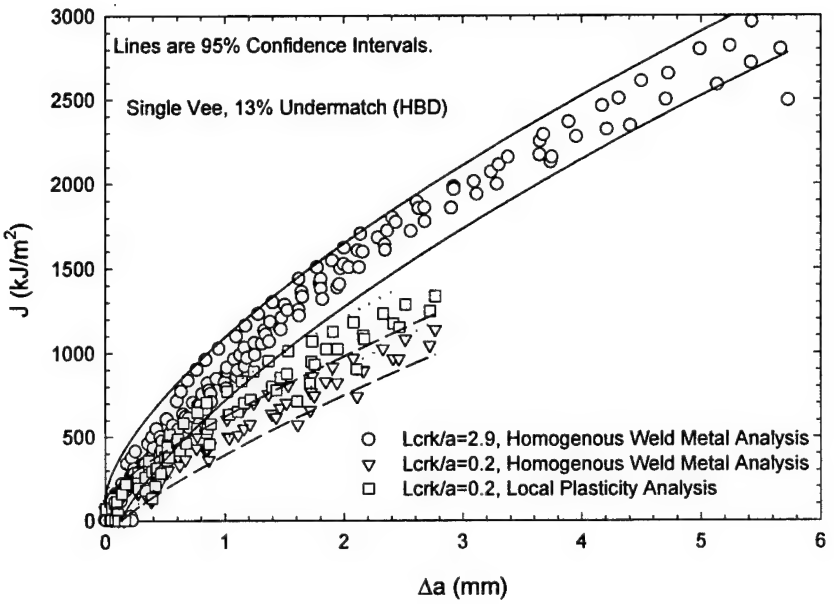

Figure 12
Crack Growth Resistance Curves for Weldment HBD

Weldment HBD, Mil-100s, single vee with weld fusion margins of 2.9 and 0.2, was investigated next. Figure 12 show the two analyses with confidence intervals for this weldment. Two remarks can easily be made from this plot. First, after accounting for the local plasticity the tearing modulus for the narrow side is still lower. While variation in tearing resistance between weld sides is not unlikely given the differences in cooling rates during welding, residual stress variation across the plate thickness and local microstructural variation between weld beads is a more probable explanation than the increased crack tip constraint. In a typical short crack bend specimen, global tensile stress/strain fields near the front face allow the local crack tip fields to relax and interact

with the free surface. A schematic of the plastic zone shapes in both deep and short crack SE(B) specimens is shown in Figure 13.

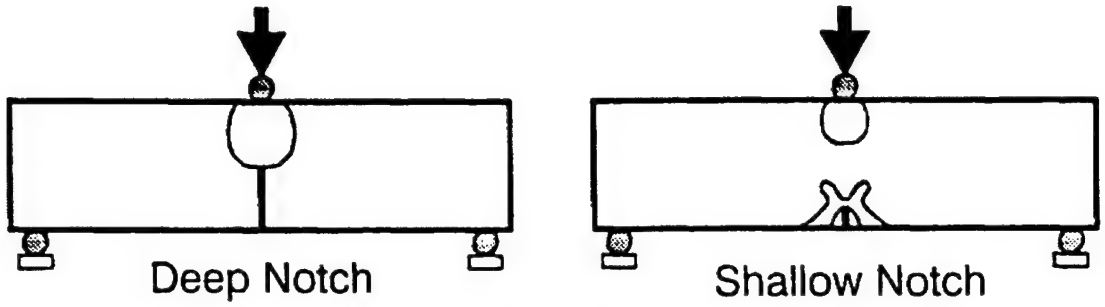

Figure 13
Schematic of Plasticity in Deep and Short Cracked SE(B) Specimens (from [40])

This quickly lowers constraint at higher deformation levels resulting is strains and stresses no longer defined by a single parameter such as J [39]. Short crack or low constraint specimens have more plasticity and lower stresses at equivalent deformation (J) levels than higher constraint specimens. This additional plastic strain influences the measured applied J and raises the crack growth resistance curve. This increase in tearing resistance has been shown in many experimental and numerical studies [19, 20, 40, 41] and is expected in homogenous specimens. However, as the higher strength baseplate impinges on the crack tip stress/strain fields and forces the plasticity away from the front face, plasticity within a short crack SE(B) approaches the fields exhibited by deeply cracked specimens. Figure 14 clearly shows the influence of the high strength baseplate containing the weld metal plasticity and funneling it though the specimen ligament. The plastic fields in this short crack specimen are now clearly highly constrained and more closely resembles the deep crack plastic zone shape illustrated in Figure 13. Therefore, using short crack homogenous equation to calculate J plainly is in error and the new η_{PL}

formulation will provide a more accurate representation of the actually J-R behavior in this specimen.

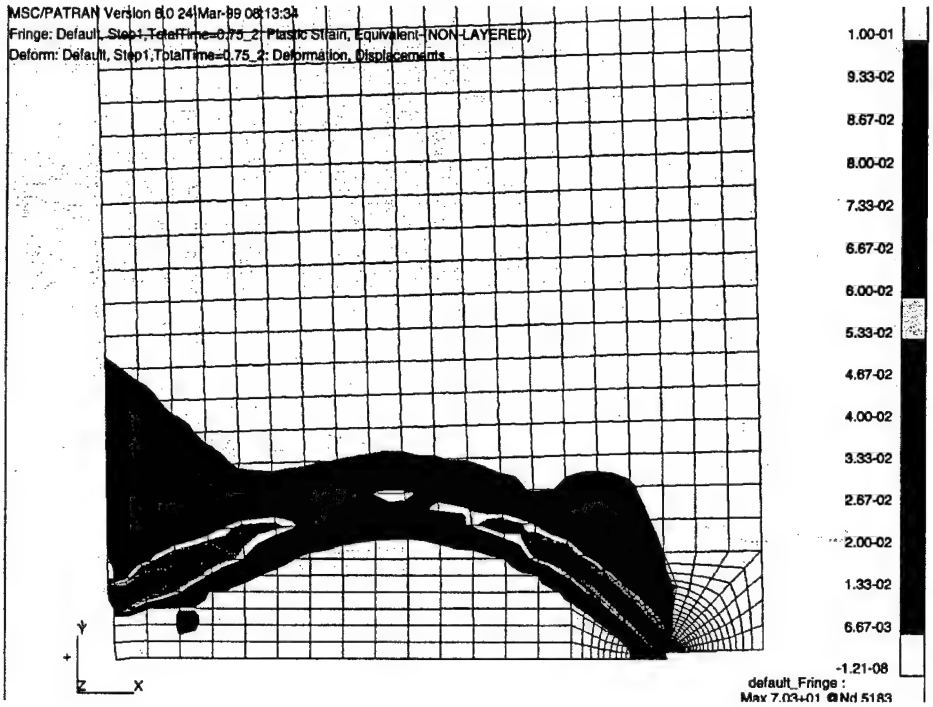

Figure 14
Finite Element Equivalent Plastic Strain Results for a/W=0.15 SE(B) Specimen with 13% Undermatched Single Vee Weld (HBD), Notch is in Narrow Side of Weld

Another discrepancy that occurs using the standard homogenous equations is in the formulation of γ in Equation 2 (repeated below). The third degree polynomial used to create Sumpter's η-factor fit may cause some of the deviation between the lower constrained (higher J-R curve) and the localized plasticity curves shown in Figure 12. Sumpter's polynomial fit for η_{PL}, shown in Figure 9 on page 19, results in strongly negative γ factors thereby raising J values calculated in Equation 1 (repeated below) and the resistance curve. Figure 15 shows the results of Equation 2 using the η_{pl}-factors defined in Figure 9.

$$J = J_{el} + J_{pl} = \frac{K^2}{E'} + \left[J_{pl(i-1)} + \frac{\eta_{(i-1)}}{b_{(i-1)}} \left(\frac{A_{pl(i)} - A_{pl(i-1)}}{B_N} \right) \right] * \left[1 - \lambda_{(i-1)} * \frac{a_{(i)} - a_{(i-1)}}{b_{(i-1)}} \right] \quad (1)$$

$$\gamma_i = \left[\eta_{pli} - 1 - \frac{b_i \eta'_{pli}}{W \eta_{pli}} \right] \quad (2)$$

The curve for Sumpter's fit begins at –4, quickly rises to –2, then begins to decreases again before jumping to positive 1 at a/W=0.282. While nothing in the mathematics in Equation 2 specifies that the γ-function should be continuous, physically the jump in the Sumpter formulation is inconsistent. The sudden jump and sign change in Sumpter's γ would mean that at a crack length of a/W=0.282, the change in J_{pl} for an increment of crack growth would also change dramatically. The γ-factors for the weldments gradually increase linearly as a/W increases with no sudden discontinuities. While the discontinuity in Sumpter's γ is troubling, none of the welded specimens reach a/W=0.282 prior to test conclusion. Regardless, the disparity between γ-functions in the two analysises may cause some of the divergence in J-R curves at higher J levels.

The homogenous analysis uses Sumpter's η and γ-factors, while the local plasticity analysis uses the results from the finite element analysis. It is clear from Equation 1 that negative γ values will increase J for an increment of crack growth and positive values will lower J. This will either raise or lower the tearing resistance results, respectively. Sumpter's γ-factor is highly negative throughout the range of a/W exhibited in the specimens tested, while the local plasticity γ-factor is positive. Therefore, for each increment of crack extension, J is adjusted up by Sumpter's γ-factor in the homogenous analysis and adjusted down slightly by the local plasticity analysis γ-factor. While these

slight adjustments are not the root cause of the differences in tearing resistance they are a contributing factor.

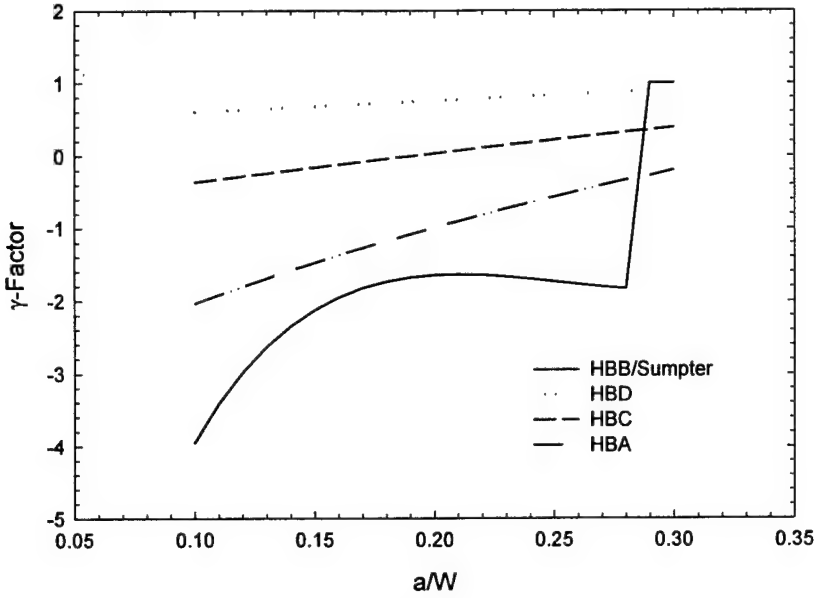

Figure 15
γ-Factors from η_{pl}-Factors in Figure 9

The second remark is illustrated better by Figure 16. This plot shows that up to initiation (J≈500 kJ/m^2) the local plasticity values are close to the values from the wide side of the weldment, resulting in consistent initiation values. Initiation values, shown in Table 8, generated from the homogenous approach deviate quickly and erroneously produce lowered values. As in weldment HBC, if only homogenous weld metal properties are used in the analysis, the results would indicate two separate behaviors near initiation. However, once the local deformation near the crack tip is included, no statistical significance can be associated with the differences at and around initiation.

These results are consistent with other published reports that J_{IC} values are relatively insensitive to constraint conditions at the crack tip [42].

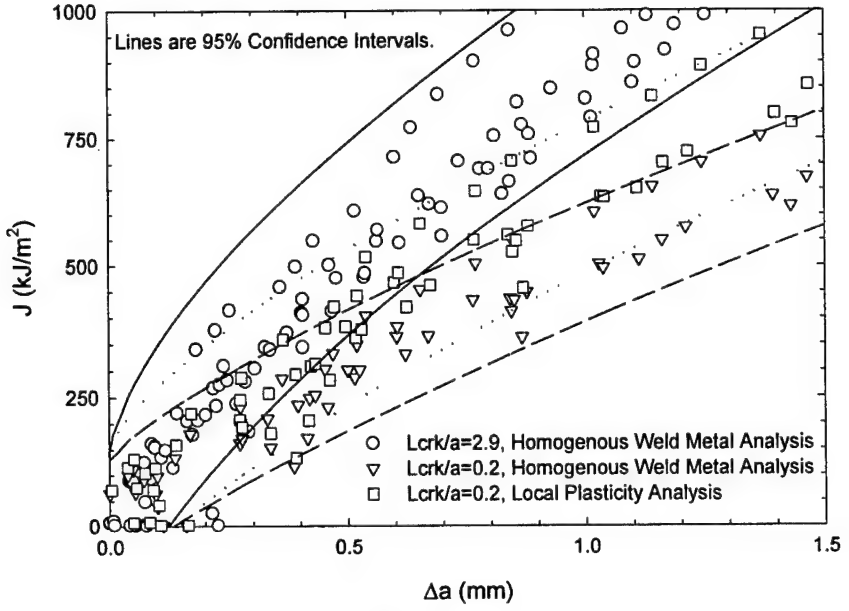

Figure 16
Crack Growth Resistance Curves Near Initiation for Weldment HBD

ID	Location	Analysis	J_{IC} (lbs/in)	J_{IC} (kJ/m²)	Valid	Comments
HBD-1	Wide	Homogenous	5853	1024	NO	Invalid Thickness
HBD-2	Wide	Homogenous	3832	671	YES	
HBD-3	Wide	Homogenous	3797	664	YES	
HBD-4	Wide	Homogenous	2772	485	YES	
HBD-5	Wide	Homogenous	3141	550	YES	
HBD-6	Narrow	Local Plasticity	2478	434	YES	
HBD-6	Narrow	Homogenous	1470	257	YES	
HBD-7	Narrow	Local Plasticity	2100	368	YES	
HBD-7	Narrow	Homogenous	1159	203	YES	
HBD-8	Narrow	Local Plasticity	3609	632	YES	
HBD-8	Narrow	Homogenous	1904	333	YES	
HBD-9	Narrow	Local Plasticity	2778	486	YES	
HBD-9	Narrow	Homogenous	1841	322	YES	
HBD-10	Narrow	Local Plasticity	1809	317	YES	
HBD-10	Narrow	Homogenous	1266	222	YES	HBD-1 Excluded
Average	Wide	Homogenous	3386	592	S.Dev.	91
Average	Narrow	Local Plasticity	2555	447	S.Dev.	122
Average	Narrow	Homogenous	1528	267	S.Dev.	59

Table 8
Initiation Toughness Values for Weldment HBD

All of the low weld fusion margin HBD specimens in this study failed due to unstable growth after significant ductile crack growth. Typically more than 2 mm of crack extension occurs prior to failure. Only one specimen with a larger weld fusion margin failed prior to test conclusion. The remaining four tests exhibited an average crack growth of more than 5.0 mm. The results, shown in Table 9, suggest that for smaller L_{crk}/a the propensity for unstable failure increases. Further, an analysis of the variance between the amount of ductile growth prior to cleavage failure or test conclusion shows statistical significance at the 95% confidence limits. Some of the variation can easily be attributed to the increased stress triaxiality in the small weld fusion margin. Unstable fracture is a stress driven event and as crack tip plasticity is constrained, stresses, including opening mode or principal stresses, increase. Obviously, factors other than fusion line proximity and constraint level influence this tendency toward unstable failure [38]. Local weld bead microstructure at the crack tip could cause local brittle zones that only specimens from the narrow side of the weld would sample resulting in the data shown in Table 9. Further investigation would be required to determine what factors determine the amount of ductile crack growth prior to instability. Moreover, as mentioned in the discussion of Charpy results (Figure 2 on page 7), these welds are not typical production welds and have a significantly higher transition temperature. Production welds would be on upper shelf at the test temperature and fully ductile behavior would be expected.

ID	Location	Δa (mm)	Fracture Mode	
HBD-1	Wide	4.0	Cleavage	
HBD-2	Wide	5.1	DNF	
HBD-3	Wide	5.4	DNF	
HBD-4	Wide	6.1	DNF	
HBD-5	Wide	6.4	DNF	
HBD-6	Narrow	2.2	Cleavage	
HBD-7	Narrow	2.4	Cleavage	
HBD-8	Narrow	3.1	Cleavage	
HBD-9	Narrow	0.8	Cleavage	
HBD-10	Narrow	2.7	Cleavage	
Average	Wide	5.4	0.94	S. Dev.
Average	Narrow	2.2	0.89	S. Dev.
DNF = Did Not Fail				

Table 9
Amount of Ductile Crack Growth Prior to Failure or Test Completion

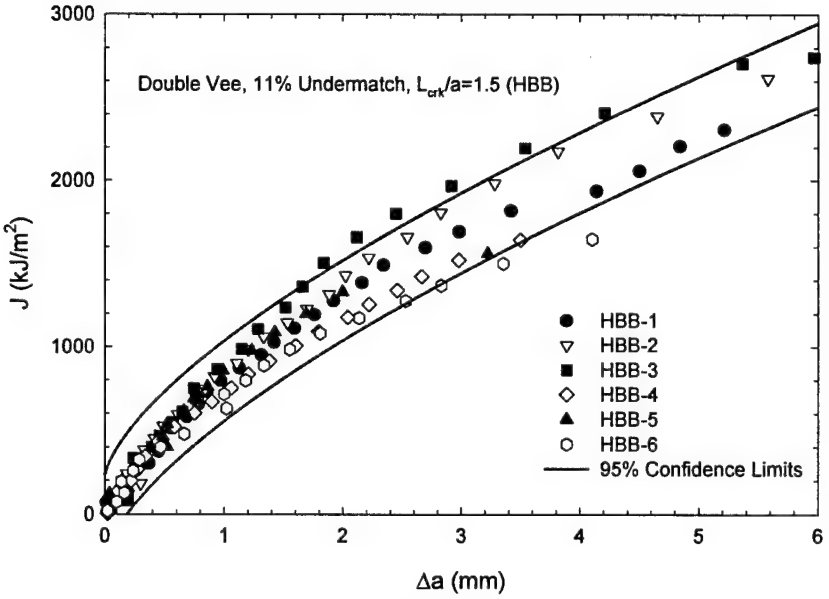

Figure 17
Crack Growth Resistance Curves for Weldment HBB

The final weldment analyzed was HBB (Mil-100s, double vee, 11% Undermatch, Lcrk/a=1.5). Figure 17 is a plot of the six resistance curves from weldment HBB, three specimens from each side of the double vee weld. Only the homogenous weld metal analysis was preformed on this weldment since L_{crk}/a was relatively large (1.5) and the

undermatching level low (-11%). Initiation, shown in Table 10, and tearing modulus from both sides of the weldment are consistent.

ID	Location	Analysis	J_{IC} (lbs/in)	J_{IC} (kJ/m^2)	Valid	Comments
HBB-1	TOP	Homogenous	3000	525	YES	
HBB-2	TOP	Homogenous	3436	601	YES	
HBB-3	TOP	Homogenous	3526	617	YES	
HBB-4	BOTTOM	Homogenous	2785	487	YES	
HBB-5	BOTTOM	Homogenous	3517	615	YES	
HBB-6	BOTTOM	Homogenous	2306	404	YES	
Average	TOP	Homogenous	3321	581	S.Dev.	49
Average	BOTTOM	Homogenous	3048	533	S.Dev.	107

Table 10
Initiation Toughness Values for Weldment HBB

Error Estimation of Homogenous Analysis

Neglecting the contribution of local plasticity and increased constraint to J_{pl} results in an under estimation of J. Figure 18 depicts the level of error as a ratio of J calculated using homogenous weld metals assumptions over J calculated with local plasticity included. These results are taken from one typical test from each of the four weldments HBA, HBC and HBD. As expected, initially the error is small, as the contribution of J_{pl} to J total is small. However, as J_{pl} becomes a larger proportion of J total, the error increases until it reaches a peak between $\Delta a/W$ of 0.01-0.02. Franco et. al have shown that variations in crack tip constraint only occur when the plastic zone physically interacts with the weld fusion line [43]. At this point plasticity begins to move away from the crack tip and out into the bulk of the remaining ligament. As the crack grows, the homogenous η_{pl} reflects the increasing crack tip constraint for the deeper crack, and the error is slowly reduced.

Two important points can be taken from Figure 18. First, errors are largest in the initial portion of the curve. This is the area where J_{IC} and tearing modulus is determined; errors in this part of the curve will result in conservative estimations of these values not representative of true material properties. Second, as the crack tip moves closer to the fusion line and the deformation level increases, the error increases dramatically. The smallest weld fusion margin shown is 0.2, which results in 20% error nearly from the outset of the test. The largest weld fusion margin in Figure 18 is 1.35. At this level errors are always less than 10%. Therefore, for L_{crk}/a larger than 1.35 errors can be ignored in all but the most exacting analysis.

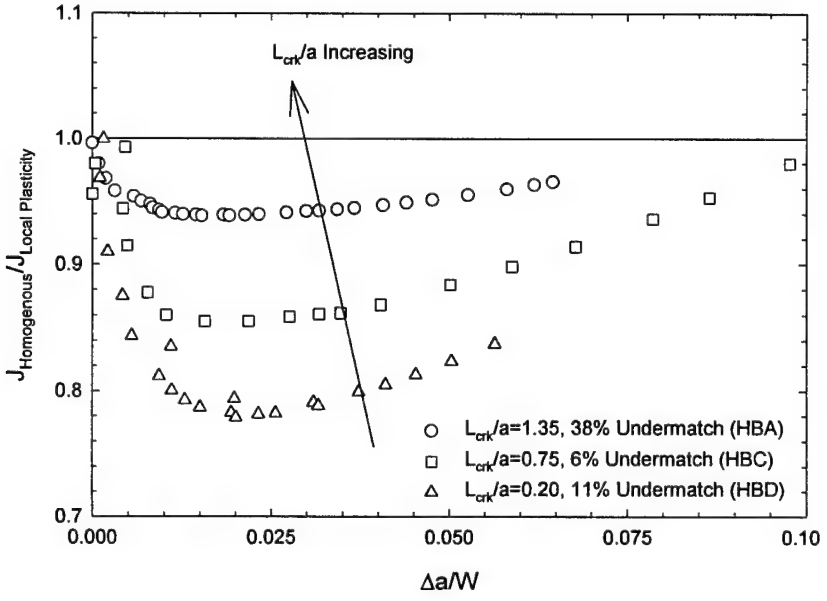

Figure 18
Under Estimation of J Using Homogeneous Weld Metal Assumption

Comparisons of J-R Curves with Various Level of Mis-Match

Crack resistance curves from three weld systems, two from this study (HBA, HBB) and one from a prior study [20] (GXL), are plotted in Figure 19. Weldment GXL is a 10% overmatched system with an L_{crk}/a of 1.8, and is composed of Mil-100s weld

consumable and HY-80 baseplate. Analysis of HBA includes local crack tip plasticity, while the analysis of GXL and HBB does not account for this effect. All three are normalized by σ_{FL}, which is defined as $(\sigma_{ys} + \sigma_{ult})/2$ and the specimen thickness, B. Clearly, once the differences in flow strength are accounted for no difference can be discerned between any of the three welds. In fact, good agreement is shown between the two Mil-100s weld systems indicating no effect from undermatching.

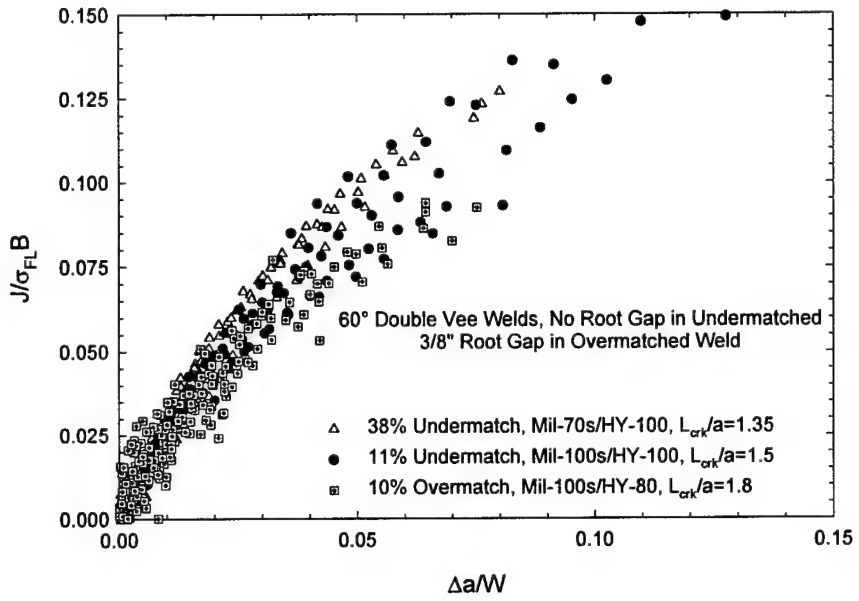

Figure 19
Normalized J-R Curves for Various Levels of Mis-Match

Weld Joint Geometry Effects

Figure 20 shows J-R curves for Mil-100s welds with a weld fusion margin greater than or equal to 1.5. These represent the wide side of the two single vee weldments (HBC, HBD) and all the tests from weldment HBB. All three sets of curves do not include local plasticity and are using homogenous weld metal as the basis for the calculation of J. Differences between data sets do not exceed typical scatter associated with toughness testing and no apparent trend in the data is evident. For joint geometries

where L_{crk}/a exceeds 1.5, toughness values appear equivalent to all weld metal toughness, and no penalty in toughness is evident from joint design.

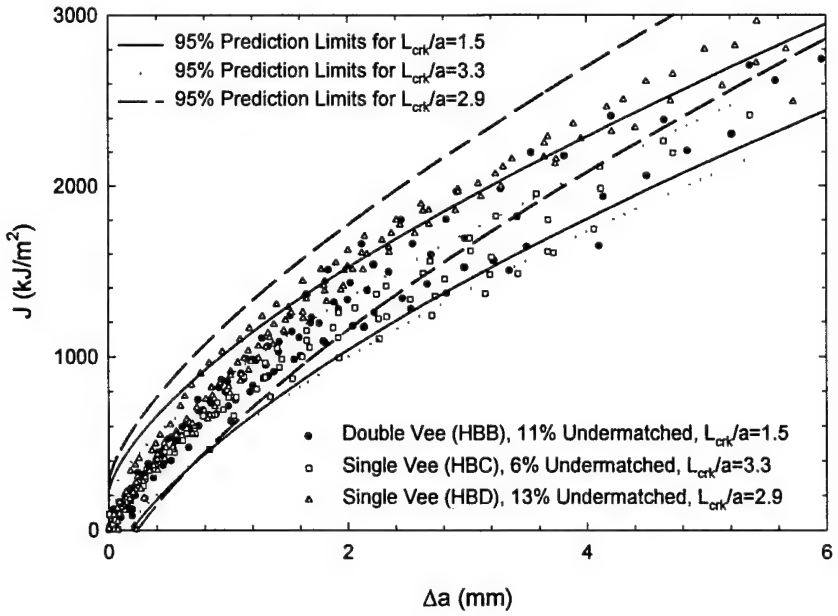

Figure 20
J-R Curves for $L_{crk}/a \geq 1.5$

Figure 21 shows J-R curves for Mil-100s welds with a weld fusion margin less than or equal to 1.5. These represent the narrow side of the two single vee weldments (HBC, HBD) and all the tests from weldment HBB. Local plasticity and constraint is accounted for in the calculation of J for both HBC and HBD. However, J calculations for HBB assume homogenous weld metal and do not account for local crack tip deformation. Significant differences in material behavior are evident at higher deformation level. However, a review of initiation values for these three data sets indicates no statistically significant differences in reported values. Scatter in J-R behavior at this level is not unexpected, especially between different weldments. As discussed previously some of the variation in toughness values may be attributed to the loss of constraint in the HBB specimens and the formulation in γ shown in Figure 15.

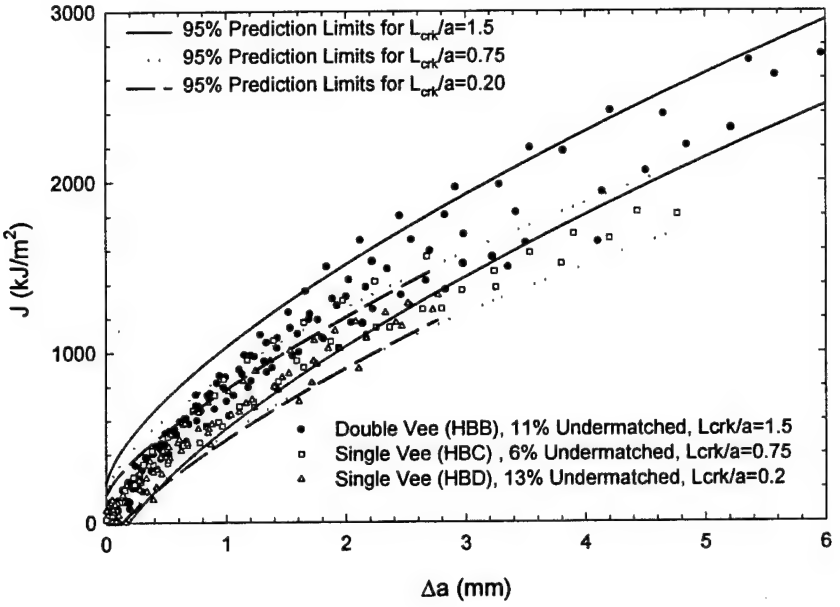

Figure 21
J-R Curves for $L_{crk}/a \leq 1.5$

Conclusion

This report investigates the effects of undermatching, joint geometry and weld fusion line margin on fracture performance of weld systems using short crack SE(B) specimens. The contributions of constraint and localized crack tip plasticity to J_{pl} are evaluated for various configurations. Calculating J in short crack SE(B) specimens assuming monolithic, homogenous weld metal properties results in J-R curves that exhibit markedly different crack growth resistance behavior and initiation toughness depending on crack tip proximity to the weld fusion line. Once local plasticity and the additional constraint caused by the weld/baseplate interface is included in the analysis, fracture behavior is independent of crack tip proximity to the fusion line up to and slightly beyond initiation. Variation in behavior beyond this point is attributed to increased constraint caused by the higher strength baseplate funneling the plastic zone through the remaining ligament. This negates the "short crack effects" that would be

expected in a homogenous specimen of similar crack length. Additional variation in fracture behavior may result from the formulation of the γ -factor used in the calculation of J_{pl} for homogenous short crack SE(B) specimens and from actual material variation within each weld.

One troubling result from this study is the apparent increased propensity for unstable fracture as the fusion line margin decreased. This result shows that a small (short) flaw in an undermatched weld located in close proximity to a higher strength material or bending field could result in a high constraint condition at the crack tip as the plastic zone was distorted. Normally, such a flaw would have the benefit of a increased tearing resistance as plasticity easily flowed to a free surface. However, in an undermatched weld the loss of constraint is neutralized and stresses increase proportionally to J in front of the crack. In this study all of the specimens with a weld fusion margin less than or equal to 0.75 failed in an unstable manner, albeit after significant prior ductile growth. As discussed previously, factors other than fusion line proximity and constraint level influence this tendency toward unstable failure. Other factors such as local weld bead microstructure at the crack tip could play a significant role. Further investigation will be required to determine what factors are at the root of these failures and determine the amount of ductile crack growth prior to instability.

It is important to note that these weldments were designed to enhance the influence of weld joint undermatching and are not production welds. This is clearly evident in the higher than expected transition temperature exhibited in charpy impact testing. Previous testing of production welds clearly indicates that transition to fully ductile behavior occurs prior to –2°C, which is the test temperature of the weldments in

this study. Unstable fracture or cleavage would not be expected from weldments displaying upper shelf behavior.

Other conclusions from this study:

- Error in calculating J using weld metal properties and ignoring the fusion line proximity at $L_{crk}/a \geq 1.5$ can be less than 10% and can reasonably be ignored.
- Errors in calculating J using weld metal properties and ignoring the fusion line proximity at $L_{crk}/a < 1.5$ can be considerable with the error increasing as the fusion line margin decreases. For L_{crk}/a of 0.2 the error can be as high as 25%. Effects of localized plasticity and increased constraint must be accounted for in the fracture analysis.
- Errors in the calculated value of J using monolithic, homogenous weld metal assumptions increase as L_{crk}/a decreases.
- Uncorrected estimates of J_{IC} in specimens where L_{crk}/a is less than 1.5 results in conservative estimations.
- Specimens with unusually steep blunting line behavior make the calculation of J_{IC} problematic. Calculation of this value becomes overly sensitive to the initial estimated crack length. It was observed that small change in the initial crack length estimate (1%) could result in large changes in J_{IC} (25%).
- ASTM 1820 crack straightness requirements are based on a percentage of average crack length, which is unduly strict for short crack specimens.
- When J values are normalized by the flow strength and thickness, J-R curves for under and over-matched welds are similar. Therefore, the effect of weld-

joint mismatch on the J-R curve can be accounted for by adjusting for the difference in flow stress.

References

1 American Society of Mechanical Engineers, Boiler and Pressure Vessel Code, Section III, Nuclear Plant Components, 1980.

2 American Welding Society, D1.1-80, Structural Welding Code, 1980.

3 MIL-STD-1688(SH), *Military Standard: Fabrication, Welding and Inspection of HY-80/100 Submarine Applications*, Washington, DC., 1981.

4 Horsley, D.J. and Glover, A.G. *"Girth Weld Strength Undermatch in High Pressure Natural Gas Pipelines,"* presented at the 2nd International Symposium on Mis-matching of Welds, Luneburg, Germany, 1996.

5 Denys, R., Lefever, T. and Glover, A. G., **"Weld Metal Yield Strength Variability in Pipeline Girth Welds,"** *Pipeline Technology*, Vol. 2, pp. 591-598, 1995.

6 Howden, et al., *"Effective Use of Weld Metal Yield Strength for HY Steels,"* National Advisory Board Report, Report No. NMAB-380, Jan. 1983.

7 Lee, M.M.K., and Luxmoore, A.R., **"An Experimental Study of the Elastic-Plastic Deformation of Double 'V' Butt Welds,"** *Journal of Strain Analysis*, Vol. 25, No. 4, pp. 255-265, 1990.

8 Luxmoore, A.R., Lee, M.M.K., and Cray, M.J., **"A Finite Element Study of Short Cracks in Mis-matched Double 'V' Welds,"** *Mis-Matching of Welds*, ESIS 17, Schwalbe and Koçak Eds., Mechanical Engineering Publications, London, pp. 614-660, 1994.

9 Cray, M.J., Luxmoore, A.R., and Sumpter, J.D.G., **"The Effect of Weld Mismatched on J and CTOD,"** *Proceedings of the Symposium on Elastic-Plastic Fracture Mechanics*, Freiburg, Germany 1989.

10 Joch, J. and Ainsworth, R. A., **"Relationship Between the J-Integral and the Crack Tip Opening Displacement for Stationary Cracks in Weldments at Plastic Collapse,"** F*atigue and Fracture on Engineering Materials and Structures*, Vol 17, pp. 1175-1185, 1994.

11 Rice, J.R., **"A Path Independent Integral and the Approximate Analysis of Strain Concentration by Notches and Cracks,"** *Journal of Applied Mechanics* , Vol. 35, pp. 379-386, 1968.

12 Kirk, M. T. and Dodds, R. H., **"Experimental J Estimation Formulas for Single Edge Notch Bend Specimens Containing Mismatched Welds,"** *Proceedings of*

the 11th International Conference on Offshore Mechanics and Arctic Engineering, Vol. 3, part B, American Society of Mechanical Engineers, pp. 439-448, 1992.

13 Gordon, J. R. and Wang, Y. Y., **"The Effect of Weld Metal Mis-Match on Fracture Toughness Testing and Analysis Procedures,"** *Mis-Matching of Welds*, ESIS 17, K. H. Swalbe and M. Koçak,, Eds., Mechanical Engineering Publications, London, pp. 351-368, 1994.

14 Burstow, M. C., Howard, I. C. and Ainsworth, R. A., **"The Effects of Material Strength Mismatching on Constraint at the Limit Load of Welded Three Point Bend Specimens,"** *International Journal of Fracture*, Vol. 89, pp. 117-142, 1998

15 Kirk, M. T. and Dodds, R. H., **"The Influence of Weld Strength Mismatch on Crack-tip Constraint in Single Edge Notch Specimens,"** *International Journal of Fracture*, Vol. 63, pp. 297-316, 1993.

16 Burstow, M. C., Howard, I. C. and Ainsworth, R. A., **"The Influence of Constraint on Crack Tip Stress Fields in Strength Mismatched Welded Joints,"** *Journal of the Mechanics and Physics of Solids*, Vol. 46, pp. 845-872, 1998.

17 Burstow, M. C. and Ainsworth, R. A., **"Comparison of Analytical, Numerical and Experimental Solutions to Problems of Deeply Cracked Welded Joints in**

Bending," F*atigue and Fracture on Engineering Materials and Structures*, Vol. 18, pp. 221-234, 1995.

18 Sumpter, J. D. G., **"J_c Determination for Shallow Notch Welded Bend Specimens,"** F*atigue and Fracture on Engineering Materials and Structures*, Vol. 10. No. 6, pp. 479-493, 1987.

19 Joyce, J. A., Hackett, E. M., and Roe, C., **"Effect of Crack Depth and Mode of Loading on the J-R Behavior of a High-Strength Steel."** *Constraint Effects in Fracture ASTM STP 1171,* E. M. Hackett, K. H. Schwalbe, and R. H. Dodds, Eds., ASTM, Philadelphia, 1993, pp. 239-263.

20 Tregoning, R. L. **"Experimental Investigation of Mismatched Weld Joint Performance,"** *Fatigue and Fracture Mechanics: 27th Volume,* ASTM STP 1296, R. S. Piascik, J. C. Newman, and N. E. Dowling, Eds., American Society for Testing and Materials, Philadelphia, 1997, pp. 427-450.

21 MIL-E23765, Military Specifications: Electrodes and Rods – Welding, Bare, Solid or Alloyed Core, Low Alloy Steel, 18 August 1987.

22 MIL-S-16216J, Military Specification: Steel Plate, Alloy, Structural, High Yield Strength (HY-80 and HY-100), 10 April, 1981.

23 ASTM E23-96, "Standard Test Methods for Notched Bar Impact Testing of Metallic Materials," 1996 Annual Book of ASTM Standards, American Society of Testing and Materials, Philadelphia, PA., 1996.

24 ASTM E8-96a, "Standard Test Methods for Tension Testing of Metallic Materials," 1996 Annual Book of ASTM Standards, American Society of Testing and Materials, Philadelphia, PA., 1996.

25 Montemarano, T. W. et al., **"Results of the Evaluation of ASTM A710 Grade A Steel Under the "Certification of HSLA Steels for Surface Ship Construction Program,"** Navy Technical Memorandum No., DTNSRDC TM-28-84-17, January 1984.

26 Lee, K.H., **"The Effect of Crack Front Curvature on Stress Intensity Factor in Compact Tension Specimens Using the Boundary Integral Equation Methods,"** The Welding Institute, Abington, England, July, 1979.

27 Towers, O.L., **"Fatigue Crack Front Shape and Its Effect on Fracture Toughness Measurement,"** *Journal of Testing and Evaluation*, Vol. 11, No. 1, pp. 34-45, 1983.

28 Towers, O. L. and Dawes, M. G., **"Welding Institute Research on the Fatigue Precracking of Fracture Toughness Specimens,"** *Elastic-Plastic Fracture Test Methods: The User's Experience, ASTM STP 856*, E. T. Wessel and F.J. Loss, Eds., American Society for Testing and Materials, Philadelphia, 1985, pp.23-46.

29 Sakano, K., **"Precompression Cracking Method for Fracture Toughness Testing – 2nd Report,"** *Ishikawijima-Harima Heavy Industries (IHI) Engineering Review*, Vol. 13, No. 3, July 1980, pp.1-7.

30 Kirk, M. T., **"A Cyclic Reverse Bending Technique for Fatigue Precracking from Shallow Notches in SE(B) Specimens,"** *Fracture Mechanics: 22nd Symposium*, Vol. 1, ASTM STP 1131, H. A. Ernst, A. Saxena and D. L. McDowell, Eds., American Society for Testing and Materials, 1992, pp.859-879.

31 M. Koçak, S. Yao and, K. H. Schwalbe, **"Effect of Welding Residual Stresses on Fatigue Precracking of CTOD Specimens,"** *Proceedings of The International Conference of Residual Stresses*, Los Angeles, CA., 8-10 August, 1989.

32 ASTM 1820-96, "Standard Test Methods for Measurement of Fracture Toughness," 1996 Annual Book of ASTM Standards, American Society of Testing and Materials, Philadelphia, PA., 1996.

33 Joyce, J. A., **"J Resistance Curve Testing of Short Crack Bend Specimens Using Unloading Compliance,"** *Fracture Mechanics: 22nd National Symposium*, Vol. 1, ASTM STP 1131, H.A. Ernst, A. Saxena, and D.L. McDowell, Eds., American Society for Testing and Materials, Philadelphia, 1992, pp. 904-924.

34 Shang-Xian Wu, Yiu-Wing Mai and Cotterell, B., **"Plastic η-Factor of Fracture Specimens with Deep and Shallow Cracks,"** *International Journal of Fracture*, Vol. 45, pp. 1-18, 1990.

35 Kirk, M.T. and Dodds, R.H., **"J and CTOD Estimation Equations for Shallow Cracks in Single Edge Notched Bend Specimens,"** U. S. Nuclear Regulatory Commission Report, NUREG/CR-5969, 1993.

36 Kumar, V., German, M. D. and Shih, C. F., *An Engineering Approach to Elastic-Plastic Fracture*, EPRI NP-1931, Electric Power Research Institute, Palo Alto, 1981.

37 Tada, H., Paris, P. C., and Irwin, G. R., *The Stress Analysis Handbook*, Paris Productions, Inc., St. Louis, 1985.

38 Zhang X.J. et al., **"SEM Stereo-Section Fractography (SSF) Observations,"** *George R. Irwin Symposium on Cleavage Fracture*, Kwai S. Chan, Ed., The Minerals, Metals & Mining Society, 1997, pp. 69-79.

39 Al-Ani, A. M. and Hancock, J. W., **"J-Dominance of Short Cracks in Tension and Bending,"** *Journal of the Mechanics and Physics of Solids*, Vol. 39, pp. 23-43, 1991.

40 Dodds, R. H., Anderson, T L. and Kirk, M. T., **"A Framework to Correlate a/W Effects on Elastic-Plastic Fracture Toughness (J_c),"** *International Journal of Fracture*, Vol. 48, pp. 1-22, 1991.

41 Sun, D.-Z., Kienzler, R., Voss, B. and Schmitt, W., **"Application of Micromechanical Models to Prediction of Ductile Fracture,"** *Fracture Mechanics: 22nd National Symposium*, Vol. 2, ASTM STP 1131, S. N. Atluri, J. C. Newman, Jr., I.S. Raju and J. S. Epstien, Eds., American Society for Testing and Materials, Philadelphia, 1992, pp. 368-378.

42 Joyce, J. A. and Link, R. E., **"Effects of Constraint on Upper Shelf Fracture Toughness,"** *Fracture Mechanics*, Vol. 26, ASTM STP 1256, W. G. Reuter, J. H. Underwood and J. C. Newman, Eds., American Society for Testing and Materials, Philadelphia, 1995.

43 Franco, C., Gilles, P., Eripret, C. and Nallet, S., **"Constraint Effects on the Upper Shelf in Cracked Welded Specimens,"** *Constraint Effects in Fracture Theory and Applications,* ASTM STP 1244, Mark Kirk and Ad Baker, Eds., American Society for Testing and Materials, Philadelphia, 1995.

DISTRIBUTION LIST

Outside Distribution

Copies	Agency
6	NAVSEA
1	SEAO3M
1	SEAO8s
1	SEA 03M2 (Null)
1	SEA 03P (McCarthy)
1	SEA 03P2 (Nichols)
1	SEA 03P4 (Manuel)
2	DTIC
4	ONR
1	1131 (Yoder)
1	1131 (Sedricks)
1	332 (Vasudevan)
1	334 (Barsoon)
1	NRL
1	Code 6310

Center Distribution

Copies	Code
1	0115 (Messick)
1	60 (Wacker)
1	601 (Morton)
1	602 (Rockwell)
1	603 (Cavallaro)
1	604 (DeSavage)
1	605 (Fisch)
1	61 (Holsberg)
1	61s
1	62 (Eichenger)
1	63 (Alig)
1	64 (Fischer)
1	65 (Beach)
1	66 (Riley)
1	67 (Hansen)
1	68 (Sudduth)
1	611 (Palko)
1	612 (Aprigliano)
1	613 (Ferrara)
1	614 (Montemarano)
1	614 (Czyryca)
1	614 (Tregoning)
1	614 (Graham)
1	614 (McKirgan)
15	614 (Mercier)
1	614s
1	615 (DeNale)
1	3421